A Preliminary Shielding Study on the Integrated Operation Verification System in the Head-End Hot-Cell of the Pyro-processing

*JINHWAN KIM[a], SEONG-KYU AHNb, YEWON KIMa, SE-HWAN PARKb, and GYUSEONG CHO**
a Department of Nuclear and Quantum Engineering, KAIST, Daejeon, Republic of Korea
b Korea Atomic Energy Reserch Institute, KAERI, Daejeon, Republic of Korea
**Corresponding author: gscho@kaist.ac.kr*

1. Introduction

Nuclear power accounts for more than 30 percent of power production in Korea. Its significance has annually been increased. Disposal spent fuel containing uranium, transuranic elements, and fission products is unavoidable byproduct of nuclear power production. it is recognized that finding appropriate sites for interim storage of disposal spent fuel is not easy because isolated sites should be required. Pyro-processing technology, Therefore, has been considered as an alternative to manage disposal spent fuel by reduction of high–level radioactive waste and the effectiveness usage of energy resources as the raw material for Sodium-cooled Fast Reactor (SFR).

As well known, pyro-processing should be operated under high radiation environment in hot-cell structures. Because of this reason, all workers should be unauthorized to access inside the hot-cell areas under any circumstances except for acceptable dose verification and a normal operation should be remotely manipulated. For the reliable normal operation of pyro-processing, it is noted that an evaluation of the space dose distribution in the hot-cell environments is necessary in advance in order to determine which technologies or instruments can be utilized on or near the process as the Integrated Operation Verification System (IOVS) is measured. According to the degree of the space dose in which the IOVS is positioned, the shielding should be also done to guarantee the IOVS performance and sustainable usage. Not like the electro-reduction and electro-refining hot-cells, the head-end hot-cell equips Camera Radiation Detector (CRD) in which plutonium is securely measured and monitored for the safeguard of the pyro-processing. Because nuclear fuel rods in the head-end hot-cell are not homogenized, the measurement of a random sample from the nuclear fuel rods should not be representative. The surveillance camera in which all processes can be monitored at once is necessary to verify the normal operation and prevent from unexpected accidents by immediate action.

Curium flux of which 244cm is an overwhelming contributor to neutron emission rate in spent fuel was calculated in the hot-cell with conceptual modeling [1]. This calculation could not reflect on the existent circumstance of the head-end hot-cell in which gamma-ray activities might overwhelm neutrons and the radiation dose from their material sources housed in the process cells effect more complicatedly on adjacent space depending on the position of the process cells.

In this paper, to verify the space dose distribution for the IOVS in the head-end process cell, effects of gamma-rays and neutrons on the space dose distribution were simulated. Furthermore, the flux and the dose which pass through the surface of the process cell from its material source were also simulated with a simplified modeling. Based on aforementioned data, a preliminary shielding study on the IOVS was calculated to meet its minimum dose requirement.

2. Model

Modeling was developed to obtain energy spectrums and to simplify the hot-cell and process cell geometries for the input data of Monte Carlo N-Particle Transport Code 6 (MCNP6). The proprietary information: batch size, process cell position and geometry were obtained from private conversation with Korea Atomic Energy Research Institute (KAERI).

2.1 Energy spectrum

The ORIGEN-ARP code was used to estimate the radionuclide inventory of the disposal spent fuel for 1 MTU of which fresh fuel composition was 4.5% ^{235}U enrichment. The average burnup was 55 GWD/MTU with 10 years cooling time. The obtained radionuclide inventory and process batch size shown in table 1 were used to get the energy spectra of gamma-rays and neutrons shown in figure 1.

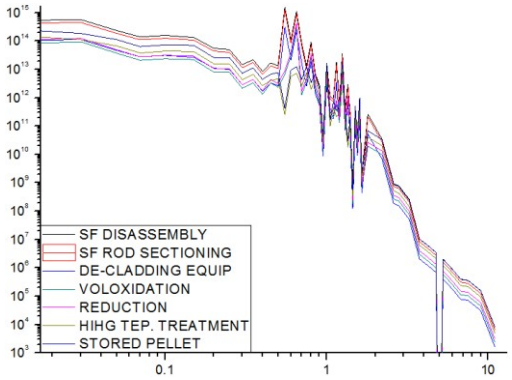

The energy spectrum of the gamma-ray

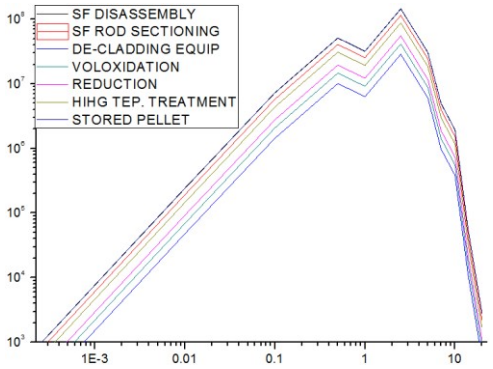

The energy spectrum of the neutron

Figure 1. Energy spectra of gamma-ray and neutron for the material sources housed in the process cells applicable to the input of MCNP6

We assumed that the energy spectra of the Work In Process 1 (WIP1), the powder mixing, the Work In Process 2 (WIP2), and the pelletizing processes were identical with the voloxidation because material sources are not chemically treated and the batch sizes are equal. The equal energy spectra are not indicated in figure 1.

2.2 Process cell modeling

Most of the process cells were simply modeled as a right circular cylinder, comprised of stainless and filled with air. SF disassembly was modeled referring to the half size of 16 × 16 array of PULS7 from Hanbit Nuclear Power Plant in Korea, comprised of zirconium cladding and filled with air. Repeated structure method: universe, fill and lattice was applied in order to simplify SF disassembly modeling. The detail specification of the process cell is indicated in table 1. and the process cell geometry applicable to mcnp6 is shown in figure 2. The height of the material source housed in the process cell was determined by its density and its radius.

2.3 Hot-cell design and geometry

The head-end hot-cell had dimensions of 12 × 71.1 × 9m, containing an air atmosphere, with 1m thickness of boron frits-baryte concrete. The hot-cell design and the position of the process cell are indicated in figure 3.

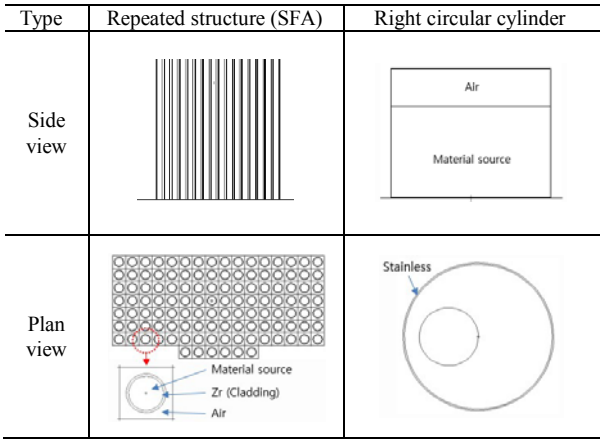

Figure 2. Process cell geometry modeling applicable to the input data of MCNP6

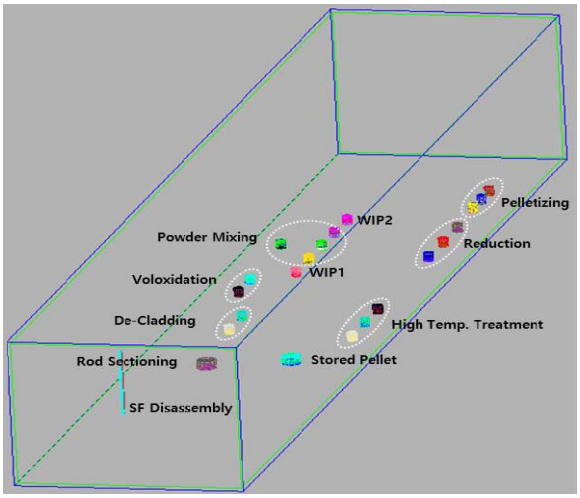

Figure 3. The hot-cell design and the position of the process cell applicable to the input data of MCNP6

Table 1. The process cell and the material source specifications applicable to the modeling for the input data of MCNP6

Process	A number of Process cell (Ea)	Material source			Process cell (cm)		
		Type	Batch size (kg)	Density (g/cc)	Radius	Height	Thickness
SF Disassembly	1	UO_2+Zr	265	10	(0.418 × 409.4 × 0.0572) × 118Ea		
Rod Sectioning	1	UO_2+Zr	250	5	50	50	0.3
De-Cladding	2	UO_2+Zr	50	7	25	50	0.3
Voloxidation	2	U_3O_8	75	2	25	50	1
WIP 1	1	U_3O_8	75	2	25	50	0.3
Powder Mixing	4	U_3O_8	75	2	25	50	0.3
WIP 2	1	UO_2	75	2.5	25	50	0.3
Pelletizing	3	UO_2	75	2.5	25	50	0.3
Reduction	3	UO_2	100	2.5	25	50	1
Stored Pellet	3	UO_2	150	2.5	25	50	1
High Temp. Treatment	1	UO_2	250	2.5	50	50	0.3

3. Result and discussion

3.1 Simulation

Results have been obtained using F2 surface tally in order to observe the magnitude of the gamma-ray and neutron flux which pass through the surface of the process cell. Furthermore, T-mesh tally has also been used to obtain the space dose distribution in the head-end hot-cell. The hot-cell was divided into 7,668 cells in which each dimension was 1 × 1 × 1m for the T-mesh tally. Both tallys mentioned above were converted into the dose rate by a flux-to-dose conversion factor by ICRP-21 and LOGLIN energy [2]. For the shielding calculations, integrated variance reduction: geometry splitting and Russian roulette, source biasing, DXTRAN, forced collision, exponential transform and weight windows was implemented to minimize a relative error and to meet the 10 statistical checks of which the results shown in this paper were completely satisfied.

3.2 The flux and the dose rate

Table 2. shows the results of the flux and the dose rate from the material source contained in each representative process cell in which the highest flux and dose rate among the same process cells was estimated. It indicates that both the magnitude of the gamma-ray flux and the dose rate were predominant rather than that of the neutron. It might be natural results, considering the gamma-ray activities were approximately 9.6E+6 times higher than that o f the neutron. The SF disassembly indicates the maximum flux and dose rate. It is believed that the highest activities of the gamma-ray and the neutron contribute to the flux and the dose rate. Furthermore, the geometry of the SF disassembly in which a relatively long height and a short radius might make the particles less attenuated in the material source itself [3]. The results of the flux and dose rate from the voloxidation and the WIP 1 suggested that the gamma-ray from the voloxidation with the 1cm thickness of stainless was more effectively attenuated rather than the WIP 3 with the 0.3cm thickness of stainless. On the other hand, the effect of the neutron on the attenuation by the stainless was not conspicuous. It is expected that the neutron flux and the dose rate indicates a seemingly small decrease because of the additional effect of the neutron multiplication [4]. The result comparison between the powder mixing and the WIP 2 shows the effect of density on the photon attenuation. The flux and the dose rate of the powder mixing with its density 2g/cm^3 was slightly higher than the WIP 2 with its density 2.5g/cm^3.

3.3 The space dose distribution

Figure 4 shows the space dose distribution of the gamma-rays and the neutron seperated by 1m height. The space dose distribution of the 1m^3 from the hot-cell inside wall is indicated in figure 5. It is typical phenomenon that the results of the space dose distribution corresponded to the results of the flux and the dose rate. The dose rate of the SF disassembly affected the adjacent space in a higher height because the 409.4cm height of the SF disassembly was modeled, whereas others were 50cm.

3.4 The position determination approach for the IOVS

To determine the position of the CRD and the surveillance camera, divergent approaches were required. Because the purpose of the CRD which contains a gamma-ray detector and a neutron detector is to identify the material composition as the process proceeds, the position in which detectable flux is exposed is required, whereas excess flux can deteriorate the performance of the CRD and shorten its usage of period. More a complex thought would, therefore, be considered for the effective shielding and detection. The surveillance camera was positioned to satisfy the two core conditions that the minimum dose rate was exposed

Table 2. The results of the flux and the dose rate which pass through the surface of the process cell in the head-end hot-cell

Process	Flux (#/cm^2/s)				Dose (mSv/h)			
	Gamma	Relative Error (%)	Neutron	Relative Error (%)	Gamma	Relative Error (%)	Neutron	Relative Error (%)
SF Disassembly	6.04E+10	1.70E-03	2.98E+04	1.40E-03	6.56E+05	1.20E-03	3.34E+01	1.40E-03
Rod Sectioning	1.65E+10	1.50E-03	1.33E+04	1.70E-03	1.63E+05	1.80E-03	1.25E+01	1.80E-03
De-Cladding	1.17E+10	2.00E-03	8.86E+03	3.40E-03	1.16E+05	3.50E-03	8.27E+00	3.60E-03
Voloxidation	7.48E+09	2.80E-03	1.27E+04	2.70E-03	7.23E+04	3.90E-03	1.23E+01	2.80E-03
WIP 1	1.09E+10	1.80E-03	1.35E+04	2.80E-03	1.17E+05	3.50E-03	1.34E+01	2.80E-03
Powder Mixing	1.10E+10	1.80E-03	1.33E+04	2.70E-03	1.18E+05	3.50E-03	1.33E+01	2.80E-03
WIP 2	9.68E+09	1.90E-03	1.31E+04	2.80E-03	1.04E+05	3.70E-03	1.29E+01	2.90E-03
Pelletizing	9.89E+09	1.90E-03	1.34E+04	2.80E-03	1.06E+05	3.70E-03	1.32E+01	2.90E-03
Reduction	8.05E+09	3.30E-03	1.66E+04	2.40E-03	7.79E+04	3.80E-03	1.59E+01	2.40E-03
Stored Pellet	1.24E+09	3.90E-03	2.70E+04	1.90E-03	1.49E+04	9.90E-03	2.60E+01	1.90E-03
High Temp. Treatment	1.32E+09	2.00E-03	1.75E+04	1.50E-03	1.63E+04	6.90E-03	1.69E+01	1.60E-03

and all processes are possibly monitored at once. The dose rate of the gamma-ray and the neutron shown in figure 5 Indicated 266 and 0.067 mSv/h respectively.

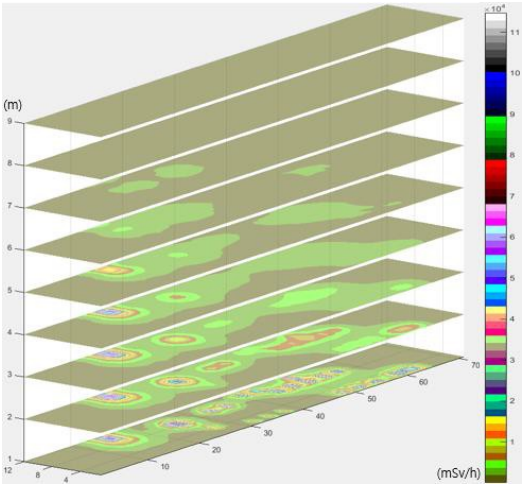

The space dose distribution of the gamma-ray

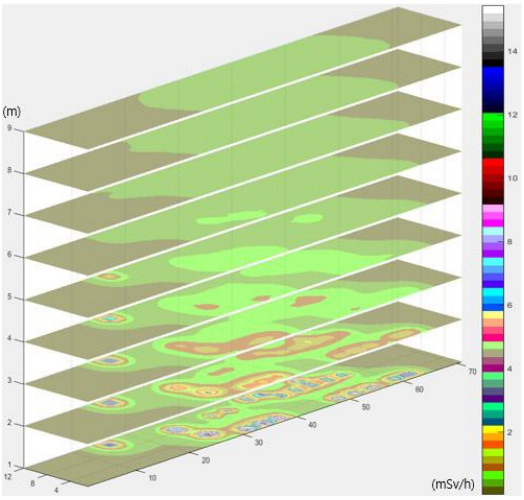

The space dose distribution of the neutron

Figure 5. The space dose distribution of the 1m3 from the hot-cell inside wall

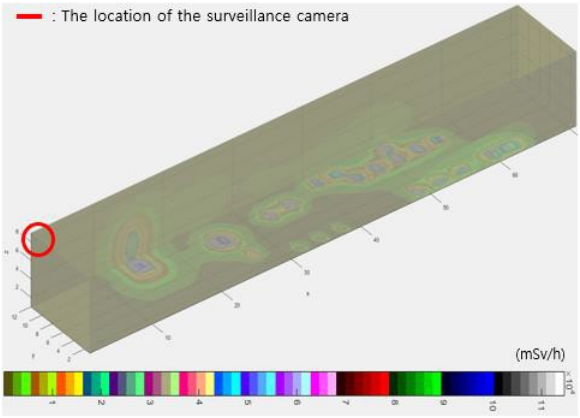

The space dose distribution of the gamma-ray

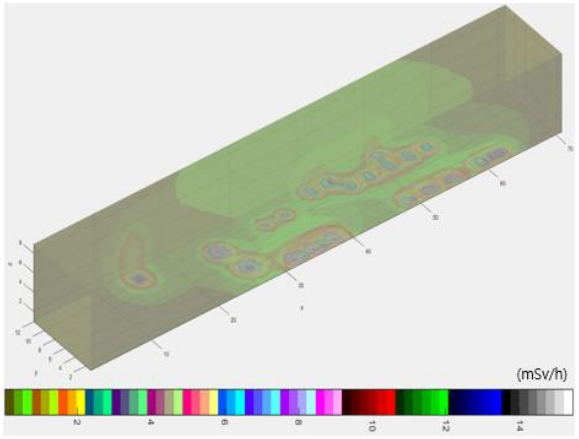

The space dose distribution of the neutron

Figure 4. The space dose distribution of the gamma-ray and the neutron seperated by 1m height

4. Future works

A preliminary shielding study on the IOVS has not yet been finished. Based on the determination of a proper position for the CRD, shielding calculation will be evaluated. Furthermore, shielding calculation for the surveillance camera will also simulated by increasing a lead thickness with integrated variance reduction methods.

REFERENCES

[1] Borrelli, R.A., Use of curium neutron flux from head-end pyroprocessing subsystems for the High Reliability Safeguards methodology, Nuclear Engineering and Design, 2014

[2] Pelowitz, Denise B. (Ed), MCNP6™ User's manual, Version 1.0, LA-CP-13-00634, 2013

[3] ROBU. E, Gamma-Ray Self-Attenuation Corrections in Environmental Samples, Romanian Reports in Physics, Vol. 61, No. 2, pp. 295-300, 2009.

[4] Sohn, H.D., Effect of Stainless Steel Plate Position on Neutron Multiplication Factor in Spent Fuel Storage Racks, Nuclear Engineering and Technology, Vol. 43, No.1, 2011.

Acknowledgement

This work was partly supported by the National Research Foundation of Korea (NRF) grant funded by the Korean government(MSIP).
(NRF-2012M2A8A5025947)